Permanent Magnet Synchronous Machine Non-Uniform Demagnetization Detection Using Zero-Sequence Magnetic Field Density

David Reigosa[*], Daniel Fernández[*], María Martínez[*], Yonghyun Park[**], Sang Bin Lee[**] and Fernando Briz[*]

[*]University of Oviedo. Dept. of Elect., Computer & System Engineering, Gijón, 33204, Spain.
[**]Korea University, Dept. of Elect. Engineering, Seoul, Korea.

diazdavid@uniovi.es, fernandezalodaniel@uniovi.es, martinezgmaria@uniovi.es, yonghyun.park@eecs.korea.ac.kr, sangbinlee@korea.ac.kr, fernando@isa.uniovi.es

Abstract: Demagnetization in permanent magnet synchronous machines (PMSMs) results in a decrease in the motor average torque and could also increase the torque ripple and consequently vibration and acoustic noise, degrading the overall performance and reliability of the drive. Demagnetization detection can be therefore of tremendous importance. Use of Hall-effect sensors has proven to be a viable option for demagnetization detection. Results reported using this method were based on the analysis of the flux density complex vector; the accuracy of this implementation strongly depends on the angle of the Hall-effect sensor, being also sensitive to implementation issues such as offsets and gain variations of the sensors, magnet temperature, manufacturing tolerances and stator current injection. This paper proposes the use of the zero-sequence component of the magnetic flux density for demagnetization detection. The use of this signal will improve the accuracy and reduce the sensitivity to implementation issues compared to the use of the flux complex vector.[1]

Keywords— Permanent magnet synchronous machines, non-uniform demagnetization, Hall-effect sensors.

I. Introduction

Design and control of PMSMs has been the focus of significant research efforts during the last three decades due to their good dynamic performance, power density and efficiency. PMs based on rare earths, e.g. Neodymium-Iron-Boron (NdFeB), are the most common option [1]-[3]. Torque production capability of PMSMs depends on the magnetization state of the PMs [1]-[2]. A decrease of the PMs magnetization state, e.g. due to temperature increase [1],[4]-[6] or to the stator current [7]-[8], results in a decrease of the motor torque and efficiency. Demagnetization can occur locally (i.e. partial demagnetization within a PM or asymmetric magnetization among poles) or globally (i.e. uniform demagnetization of all PMs) [9]-[10]. Global demagnetization typically results in a decrease of the average

torque; local demagnetization can also produce an increase of the torque ripple, motor vibration and acoustic noise [32]. PM demagnetization detection in PMSMs is therefore of great importance.

Magnetization state can be measured by inserting a gauss meter in the machine air gap [10]-[11]; removing or drilling the end frame of the machine is required to insert the field sensor, field measurement being feasible only with the machine at standstill. Use of field sensors inserted between PMs and rotor lamination was proposed in [12]. Combined with a wireless transmission of the signal, this system provides real time measurement of the magnetization state and without interfering with the normal operation of the machine. Unfortunately this solution is expensive and compromises the robustness of the drive, being therefore unacceptable in most applications.

Alternatively to direct measurement, PM magnetization state can be estimated. Global [13]-[18] and local [18]-[26] demagnetization detection/estimation methods have been already proposed. Global demagnetization estimation can be performed using BEMF [13]-[14], signal injection [15]-[17] and Hall-effect sensor [18] based methods. BEMF and signal injection methods estimate the magnetization state from stator terminal variables; BEMF requires the machine to be rotating, estimation at low speed or standstill not being possible. On the other hand, signal injection methods place concerns because of the potential adverse effects (additional noise, vibration and losses) due to the injected signal. Local demagnetization estimation methods include stator current analysis [19]-[20], zero-sequence voltage [21], BEMF [22], vibration analysis [23]-[24], change in the shaft trajectory [25], signal injection [26] and Hall-effect sensors [18], [31]. Stator current analysis, zero-sequence voltage, BEMF, vibration analysis and changes in the shaft trajectory methods require the machine to be rotating; signal injection methods require the machine to be at standstill, with the disadvantage of requiring the injection of an additional signal; as for the global demagnetization case.

Demagnetization detection using Hall-effect sensors was proposed in [18]. Hall-effect sensors already present in many PMSM drives for magnet polarity and initial position detection [27]-[29] can be used for indirect measurement of the PM flux, enabling detection of partial and global magnetization at any speed and without interfering with the normal operation of the machine. The implementation

proposed in [18] was based on the analysis of the magnetic flux density complex vector. A conclusion of that work was that measuring the flux in the radial direction is preferred over measurements in the tangential or axial directions in terms of reliability/sensitivity requirements. In addition, the method was demonstrated to be sensitive to several implementation issues, being the most relevant: offsets in the sensors, unbalances in sensors' gains, manufacturing tolerances, stator current effects and magnets' temperature.

This paper proposes the use of the zero-sequence component of the magnetic flux density for demagnetization detection. It will be shown that the use of the zero-sequence component significantly reduces the sensitivity to several implementation issues, including sensors location, DC offsets and gain variations of the sensors, PMs' temperature or stator current injection. Potential uses of the proposed technique include machine condition monitoring, development of torque ripple compensation techniques or improving existing torque ripple minimization techniques, e.g. [33]-[36].

The paper is organized as follows: Magnetic flux density measurement and zero-sequence component calculation in PMSMs is discussed in section II; zero-sequence magnetic flux density modeling of a partially demagnetized PM is described section III; experimental verification of non-uniform demagnetization detection using the zero-sequence magnetic flux density is discussed in section IV; discussion on implementation issues is included in section V; conclusions are finally presented in section VI.

II. Magnetic flux density measurement and zero-sequence component calculation in PMSMs

This section discusses the measurement and processing of the zero-sequence magnetic flux density component. Schematic design of the machine is shown in Fig. 1a and 1b. The machine is equipped with Neomax 42-SH PMs. Dimensions and ratings of the test machine are shown in Table I. Hall-effect sensors are attached to the end shield as shown in Fig. 1c, i.e. the sensor is placed between the rotor and end shield. Assembly of the sensors and connection to the control board does not differ from arrangements in standard drives for different purposes (encoder/resolver, digital-hall-effect sensors, thermal sensors mounted in the stator of the machine,…). The end shield was modified to allow insertion/extraction of the PMs without the need of removing the rotor/end shield (rectangular window in Fig. 1d).

| Table I. Machine parameters	
P_{RATED} (kW)	7.5
I_{RATED} (A)	14
ω_{RATED} (rpm)	1800
Stator slots	36
Poles	6
Rotor radius (mm)	54.2
Magnets	N42 SH
Magnet dimensions: width, height and length (mm)	42x6x10
Magnet position from shaft center (mm)	44.6

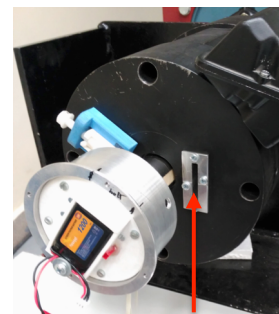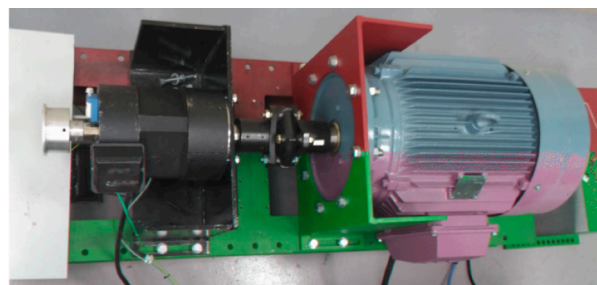| Sensor position:	
• Radius (mm)	44.6
• Distance from the rotor in axial direction (mm)	5
Airgap length (mm)	0.8
Inner stator radius (mm)	55
Outer stator radius (mm)	88

a)

b)

c)   d)   window
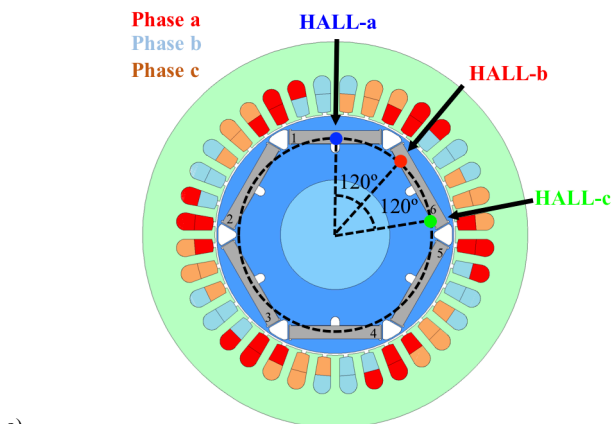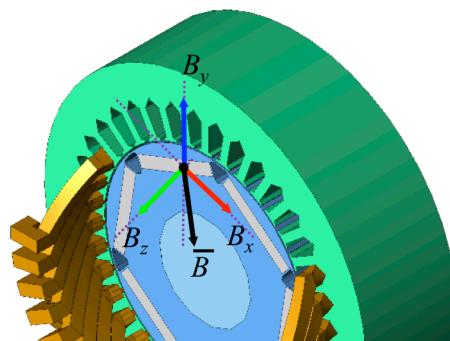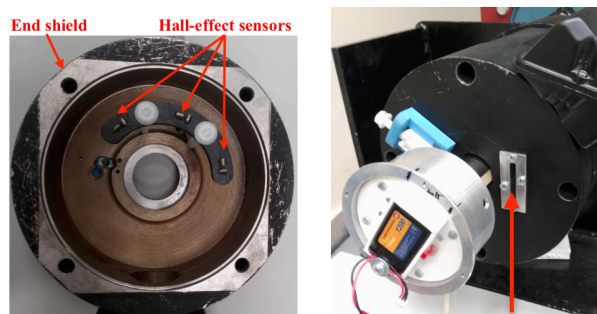
e)

Fig. 1.- Machine desing and experimental setup. a) 2D and b) 3D schematic representation of the machine and sensors location; x, y and z correspond to the tangential, radial and axial directions respectively. c) Machine end shield with the Hall-effect sensors, d) machine shield modification for easy PM replacement, and e) test bench.
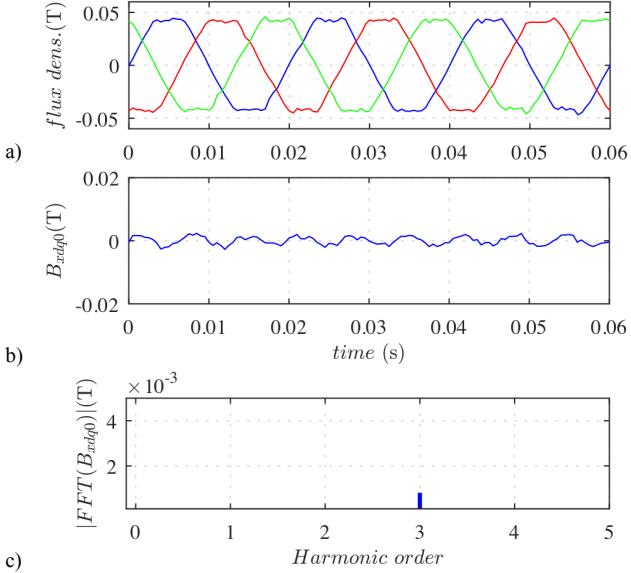
Fig. 2.- a) flux density measurements in the x-axis direction by the three analog Hall effect sensors (B_{xa} , B_{xb} and B_{xc}), b) resulting zero-sequence magnetic flux density, B_{xdq0} ,c) and FFT of B_{xdq0} . ω_r=1pu and i_{dq}=0pu.
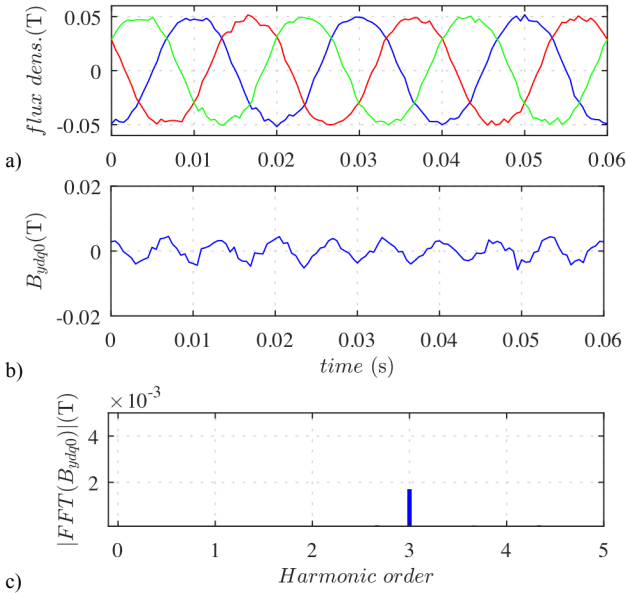

Fig. 3.- Same results as in Fig. 2 for the y-axis direction.

Previous to insertion in the rotor, PMs are magnetized/demagnetized using a pulse magnetizer [16]-[18]. Fig. 1d shows the test bench, which consists of the test machine and a load machine. Standard Hall-effect sensors used in PMSMs drives for motion control [30] will be used in this work. Though practical implementation of the method would use standard 1D sensors, an arrangement of three sensors able to measure along x, y and z (radial, tangential and axial) directions have been developed to analyze the influence of measurement angle.

The zero-sequence magnetic flux density is defined by (1), where m stands for x, y or z-axis and B_{ma}, B_{mb} and B_{mc}, are the magnetic flux densities measured by sensors a, b and c along the m direction respectively.

$$B_{mdq0} = 1/3\left(B_{ma} + B_{mb} + B_{mc}\right) \qquad (1)$$

An example of the measured magnetic flux density along the x-axis direction for one rotor revolution is shown in Fig. 2a. Fig. 2b shows the resulting zero-sequence magnetic flux density, B_{xdq0}, while Fig. 2c shows the FFT of B_{xdq0}. Since the measured zero sequence flux density must be a periodic function over a whole mechanical revolution, its frequency spectrum can be expressed as (2), where ω_r is the machine speed, and $B^s_{mdq0\_n\omega r}$ and φ_{nm} are the magnitude and phase of the "n^{th}" harmonic component.

$$B_{mdq0} = \sum_n B_{mdq0\_n\omega r} \sin\left(n\omega_r t + \varphi_{nm}\right) \qquad (2)$$

It is observed from Fig. 2c that the main harmonic component of B_{xdq0} is a third harmonic. Fig. 3 shows similar results as Fig. 2 but when the field is measured along y-axis direction; measurements in both axes are seen to behave very similar.

It is finally noted that, from the experimental results obtained in this work, the flux density in the z-axis direction is significantly smaller compared to x and y-axis for the specific case where the sensor is located at x=y=0 mm (see Table I). Since this prevents reliable detection of demagnetization, measurements in the z-axis will not be therefore discussed further.

III. Zero-sequence magnetic flux density modeling of a partially demagnetized PM

It is useful for analysis purposes to develop models able to predict the effect of demagnetization of the flux measured by the sensors, "ANSYS-Maxwell" software has been used for this purpose [37]. Fig. 4a and Fig. 5a show the ideal flux measured by the three analog Hall-effect sensors (B_{ma} , B_{mb} and B_{mc}) in the x and y-axis directions respectively for the case of an ideal machine (i.e. purely sinusoidal waveforms). These ideal results agree with the experimental results shown in Fig. 2 and Fig. 3. Higher-order harmonics observed in the experimental results, see Fig. 2 and Fig. 3, are due to the non sinusoidal distribution of the flux in a real machine. Fig. 4b and Fig. 5b show the corresponding zero-sequence magnetic flux densities, B_{mdq0} (1), for the x and y-axis directions respectively. In case of a demagnetized PM, the flux measured by the Hall-effect sensors will not be sinusoidal anymore but shaped by the demagnetized PMs. Such shaped flux measurements can be modeled as the product of the signals shown in Fig. 4a and Fig. 5a by a window function. The value of this window function is 1 when healthy PMs face the sensor and <1 if demagnetized PMs face the sensor. Window functions for sensors a, b and c (W_{ma} ,W_{mb} and W_{mc}) will be shifted by 120 electrical degrees, which is the physical angle between adjacent sensors. More precise window functions could be defined using stator and rotor design information, e.g.

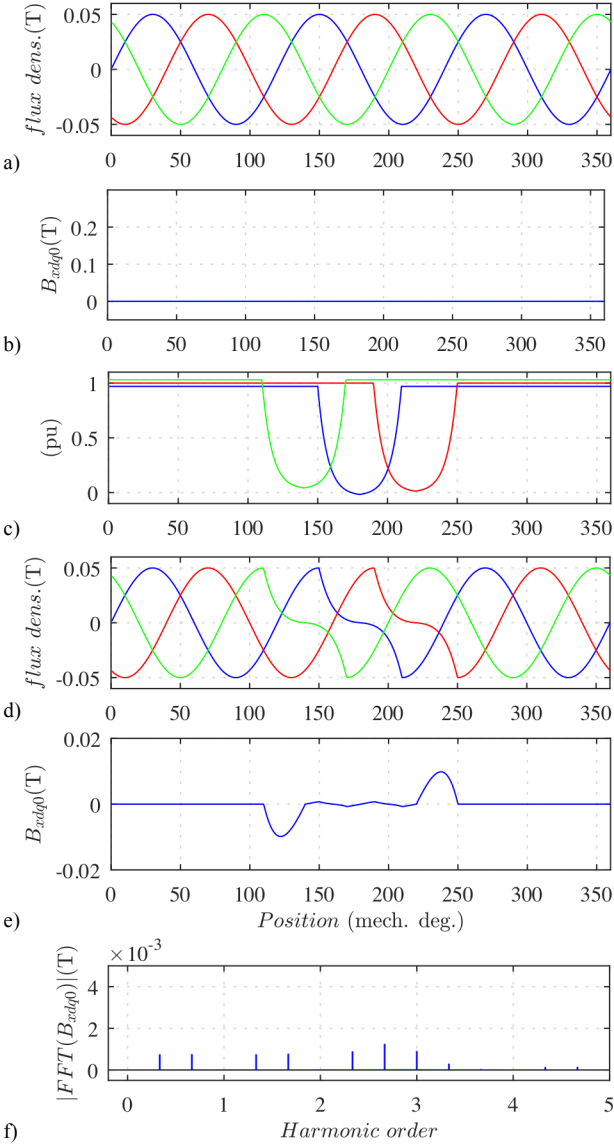magnet shape, magnet layers, flux barriers, stator teeth design, etc.

a)

b)

c)

d)

e)

f)

Fig. 4.- a) Theortical flux density in the x-axis direction by the three hall-effect sensors (B_{xa} , B_{xb} and B_{xc}) in a healthy machine, b) zero-sequence magnetic flux density, B_{xdq0} , resulting from the waveforms shown in a), c) profile of flux density variation due to demagnetization (1 PM demagnetized by 50%), d) modeled flux density in the x-axis direction due to demagnetization obtained by multiplying the theoretical flux density in a) by the window functions in c), e) zero-sequence magnetic flux density, B_{xdq0} , resulting from the waveforms shown in d), and f) FFT of B_{xdq0} shown in e). Machine operating condition: ω_r=1pu and i_{dq}=0pu.

Such window functions will be identical for sensors *a*, *b* and *c* but shifted by 120 electrical degrees. Windows functions of the type shown in Fig. 4c and Fig. 5c have been found to fit well with experimental measurements.

Fig. 4d and Fig. 5d show the flux densities that result from multiplying the flux measurements shown in Fig. 4a and Fig. 5a by the window functions in Fig. 4c and Fig. 5c (W_{ma}, W_{mb} and W_{mc}), (3)-(5). Fig. 4e and Fig. 5e show the zero-sequence

component of flux density, B_{mdq0} (6), resulting from the flux densities shown in Fig. 4d and Fig. 5d.

$$B'_{ma} = B_{ma}W_{ma} \tag{3}$$

$$B'_{mb} = B_{mb}W_{mb} \tag{4}$$

$$B'_{mc} = B_{mc}W_{mc} \tag{5}$$

$$B_{mdq0} = 1/3\left(B_{ma}W_{ma} + B_{mb}W_{mb} + B_{mc}W_{mc} \right)$$
$$= 1/3\left(B'_{ma} + B'_{mb} + B'_{mc} \right) \tag{6}$$
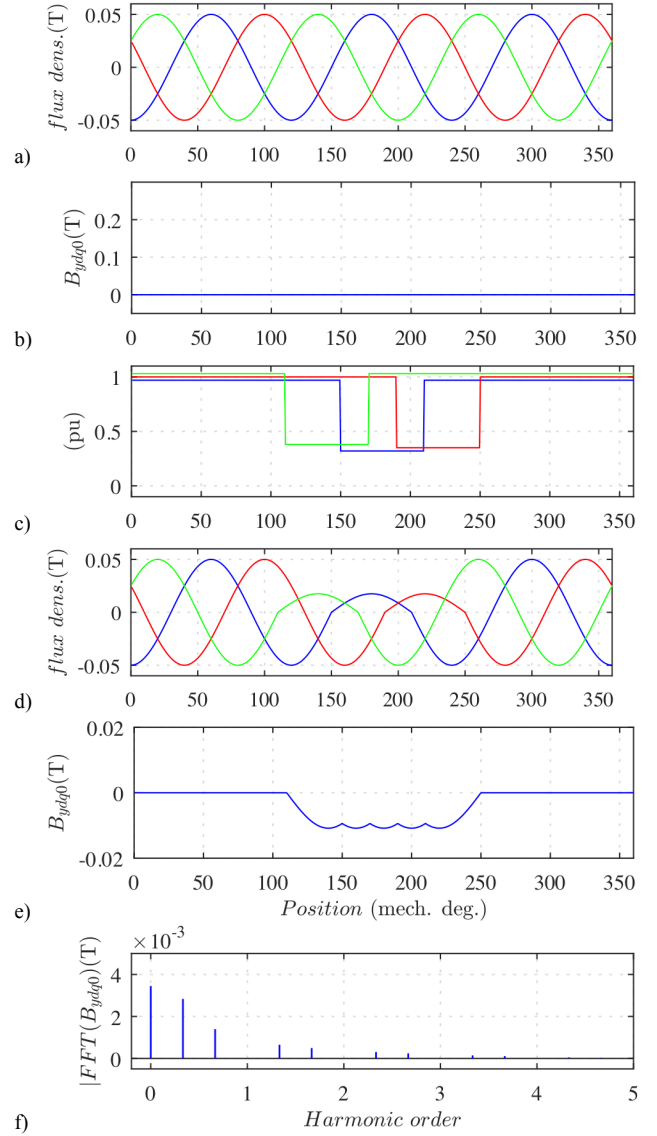
a)

b)

c)

d)

e)

f)

Fig. 5.- Same results as in Fig. 4 for the y-axis direction.

Different metrics can be defined, either in the time domain or in the frequency domain, from the processing of the zero sequence flux to assess PM condition. Simple metrics in the time domain include the mean value and peak-to-peak value of the zero sequence flux (see Fig. 4e and 5e). In case of performing the analysis in the frequency domain, it is observed from Fig. 4f and Fig. 5f that demagnetization of PMs induces additional harmonic components in the spectrum of

B_{mdq0}. Tracking of such harmonics can be used to assess PM condition.

IV. Experimental verification of non-uniform demagnetization detection using the zero-sequence magnetic flux density
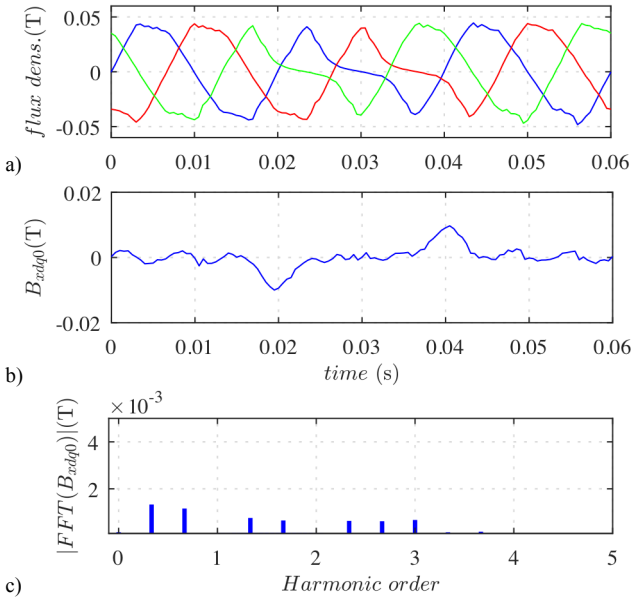

a)

b)

c)

Fig. 6.- a) flux density measurements in the *x*-axis direction by the three analog Hall effect sensors (B_{xa}, B_{xb} and B_{xc}), b) resulting zero-sequence magnetic flux density, B_{xdq0}, and c) FFT of B_{xdq0}. Machine operating condition: ω_r=1pu and i_{dq}=0pu, 1 PM demagnetized by 50%.
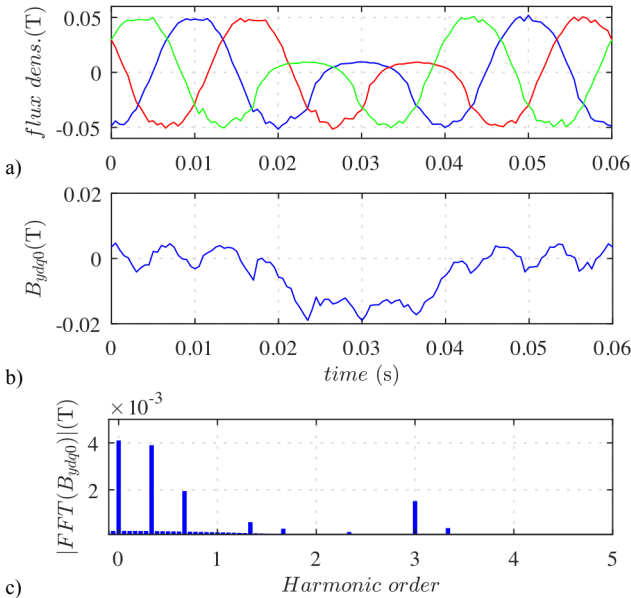

a)

b)

c)

Fig. 7.- Same results as in Fig. 6 for the *y*-axis direction.

Fig. 6 and Fig. 7 show experimental results when one of the PMs of the test machine (PM #4 in Fig. 1) is demagnetized by 50% when the flux is measured in the *x* and *y*-axis directions. It can be observed that the measurements in Fig. 6a and Fig. 7a are in good agreement with the patterns shown in Fig. 4d and

Fig. 5d. Fig. 6c and Fig. 7c show the FFTs of the zero-sequence flux, which are also seen to be in good agreement with the predictions shown in Fig. 4f and Fig. 5f.

Fig. 8a and Fig. 8b show the variation of different metrics using the flux zero sequence when the demagnetization of PM #4 goes from zero (fully magnetized PM) to 50%. Fig. 8a shows the mean value of B_{mdq0} and $\left|B_{mdq0}\right|$ as demagnetization degree of PM #4 increases. As expected, the mean value of B_{xdq0} is not useful as it is a symmetric waveform (see Fig. 6a). On the other hand, mean values of $\left|B_{xdq0}\right|$, B_{ydq0} and $\left|B_{ydq0}\right|$ change almost linearly with the demagnetization state, allowing reliable demagnetization detection even for low demagnetization levels. Fig. 8b shows the peak-to-peak of B_{mdq0} and $\left|B_{mdq0}\right|$ both signals being also almost a linear function of the demagnetization degree.

a)

b)

Fig. 8.- a) mean and b) peak-to-peak of the zero-sequence magnetic flux density, B_{mdq0}, and absolute value of the zero-sequence magnetic flux density, $\left|B_{mdq0}\right|$, vs. PM #4 demagnetization level. Machine operating condition: ω_r=1pu and i_{dq}=0pu.

Fig. 9 shows the variation of the same metrics shown in Fig. 8 but when the number of demagnetized PMs increase: PMs are demagnetized sequentially from PM #1 to #6, see Fig. 1; magnetization state of demagnetized PMs being set to 80%. As expected from Fig. 8a, the mean value of B_{xdq0} is not useful for demagnetization detection. It is observed that the mean value of B_{ydq0} is higher when the number of demagnetized PMs is odd than when it is even; this is explained because when the number of demagnetized PMs is even, a complete pole pair is demagnetized, B_{ydq0} waveform being therefore symmetric, as expected from Fig. 5. It can be therefore concluded that mean value of B_{ydq0} is a reliable metric to distinguish faults which affect to a complete pole or pole pair.

Mean values of $\left|B_{xdq0}\right|$ and $\left|B_{ydq0}\right|$ are almost zero when there are no demagnetized PMs or when the demagnetization is uniform, i.e. uniform demagnetization cannot be distinguished using this metric. In addition, both are seen to
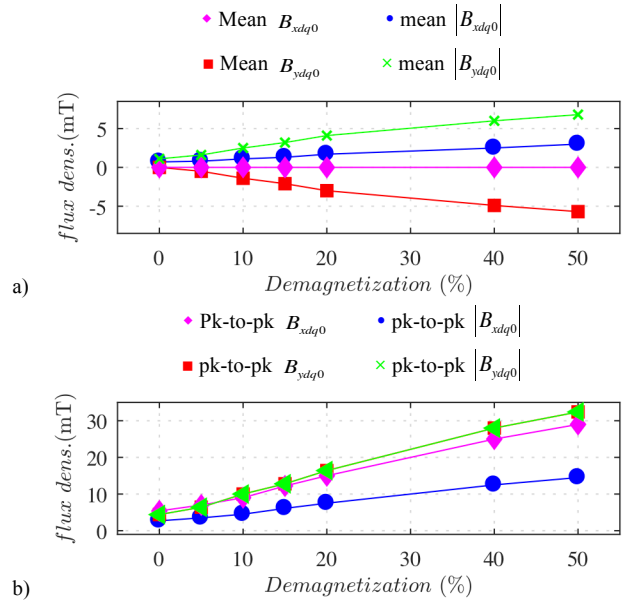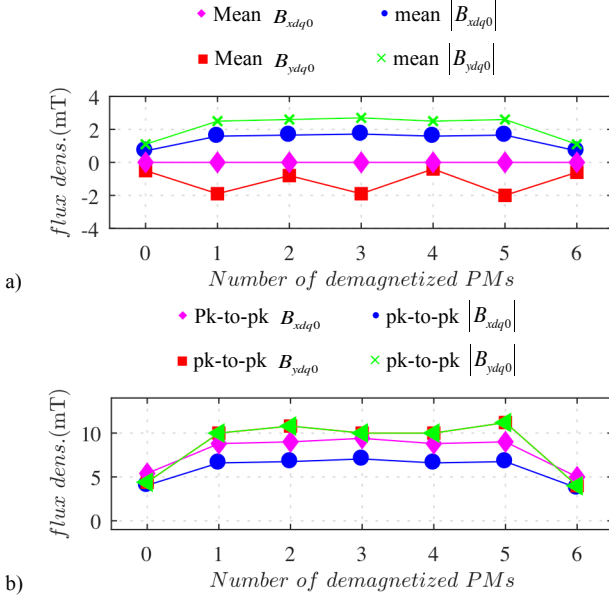
Fig. 9.- a) mean and b) peak-to-peak of the zero-sequence magnetic flux density, B_{mdq0}, and absolute value of the zero-sequence magnetic flux density, $\left|B_{mdq0}\right|$, vs. number of demagnetized PMs (magnetization level=90%). Machine operating condition: $\omega_r=1$pu and $i_{dq}=0$pu.

be almost independent of the number of demagnetized magnets. It is concluded that these are reliable metrics of the demagnetization degree (see Fig. 8a), but fail to show the number of PMs that have been demagnetized.

It is observed from Fig. 9b that the peak-to-peak value of B_{mdq0} and $\left|B_{mdq0}\right|$ shows a relative small value when the number of demagnetized PMs is 0 or 6, i.e. uniform demagnetization cannot be distinguished using this metric. It is also observed from Fig. 9b that the peak-to-peak of B_{mdq0} and $\left|B_{mdq0}\right|$ show almost no dependence on the number of demagnetized magnets. Consequently, they can be a reliable metric for the demagnetization degree (see Fig. 8b), but not of the number of PMs demagnetized.

Table II summarizes the properties of the different metrics. Refinement of these metrics is a subject of ongoing research.

Table II. Metrics to detect demagnetization					
	Uniform demag.	Non-uniform demag.	Asymmetries among poles	Asymmetries among pole pairs	Demag. degree
Mean B_{xdq0}	✗	✗	✗	✗	✗
Mean $\left|B_{xdq0}\right|$	✗	✔	✗	✗	✔
Mean B_{ydq0}	✗	✔	✔	✗	✔
mean $\left|B_{ydq0}\right|$	✗	✔	✗	✗	✔
Pk-to-pk B_{xdq0}	✗	✔	✗	✗	✔
Pk-to-pk $\left|B_{xdq0}\right|$	✗	✔	✗	✗	✔
Pk-to-pk B_{ydq0}	✗	✔	✗	✗	✔
Pk-to-pk $\left|B_{ydq0}\right|$	✗	✔	✗	✗	✔

V. Implementation issues

The performance of the proposed method can be affected by several implementation issues, including: 1) sensors DC offsets, 2) sensors gains unbalances; 3) manufacturing tolerances; 4) stator current effects; 5) magnets' temperature. All these issues are analyzed following.

V.A. Sensors DC offsets

DC Offsets in the sensors measurements (ΔB_{ma}, ΔB_{mb}, ΔB_{mc}) can be modeled as shown in (7). It can be observed from (7) that they induce a DC component in B_{mdq0}, i.e. $1/3(\Delta B_{ma}+\Delta B_{mb}+\Delta B_{mc})$.

$$
\begin{aligned}
B_{mdq0} &= 1/3\begin{pmatrix} (B_{ma}+\Delta B_{ma})+(B_{mb}+\Delta B_{mb})+ \\ (B_{mc}+\Delta B_{mc}) \end{pmatrix} = \\
&= 1/3(B_{ma}+B_{mb}+B_{mc})+ \\
&\quad +1/3(\Delta B_{ma}+\Delta B_{mb}+\Delta B_{mc})
\end{aligned}
\tag{7}
$$

Fig. 10 shows the magnetic flux density measurements along y-axis by Hall sensors aligned with phases a, b and c, the resulting zero-sequence magnetic flux density, B_{ydq0}, and the FFT of B_{xdq0}, when Hall sensor "a" (see Fig. 1) has an offset of 0.1pu and one of the PMs of the test machine (PM #4 in Fig. 1) is demagnetized by 50%.

It can be observed from Fig. 10 that ΔB_{ya} (i.e. offset of Hall sensor "a") results in an offset in B_{ydq0}. If the metric used to detect demagnetization is the mean value of B_{ydq0} or $\left|B_{ydq0}\right|$, offsets in the sensors measurements will compromise the accuracy; a pre-commissioning stage to calibrate the sensors would be therefore required. On the contrary, if demagnetization detection is based on the peak-to-peak variation respect to the healthy case, offsets in the sensors would have no influence.

It must be noted however that DC offsets will be relevant if demagnetization detection is based on the absolute value, e.g. mean value of B_{ydq0} or $\left|B_{ydq0}\right|$. On the contrary, if demagnetization detection uses variation with respect to the healthy case, offsets in the sensors are not expected to affect.

V.B. Sensors gains unbalances

Unbalances in sensors' gains (Δk_a, Δk_b and Δk_c) can be modeled as (8); which can be also expressed as (9). It can be observed from (9) that unbalances in the gains will result in an additional harmonic component, i.e. $\Delta B_k \sin(\omega_r t + \varphi_{\Delta k})$, that oscillates at the machine speed (ω_r); where ΔB_k and $\varphi_{\Delta k}$ are the magnitude and phase of the harmonic component due to variations in the sensors.

$$
B_{mdq0} = 1/3\begin{pmatrix} (1+\Delta k_a)B_{ma}+(1+\Delta k_b)B_{mb}+ \\ (1+\Delta k_c)B_{mc} \end{pmatrix}
\tag{8}
$$

$$
\begin{aligned}
B_{mdq0} &= 1/3(B_{ma}+B_{mb}+B_{mc}) \\
&\quad +1/3(\Delta k_a B_{ma}+\Delta k_b B_{mb}+\Delta k_c B_{mc}) \\
&= 1/3(B_{ma}+B_{mb}+B_{mc})+\Delta B_k \sin(\omega_r t+\varphi_{\Delta k})
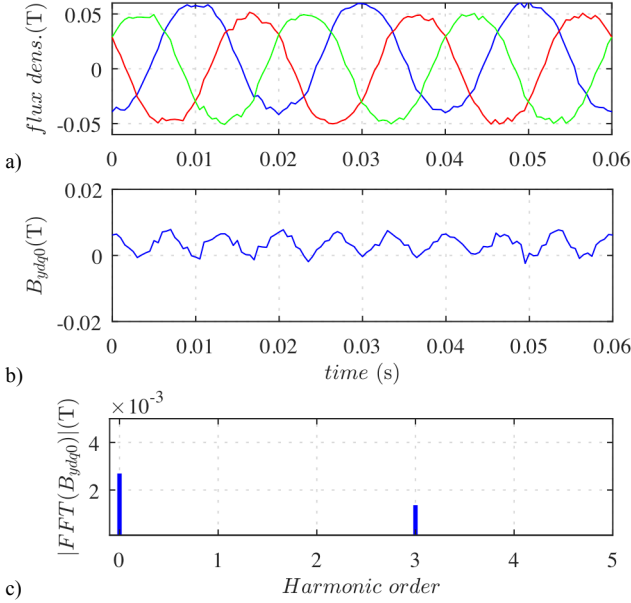\end{aligned}
\tag{9}
$$

Fig. 10.- a) flux density measurements in the *y*-axis direction by the three analog Hall effect sensors (B_{ya} , B_{yb} and B_{yc}), b) resulting zero-sequence magnetic flux density, B_{ydq0} , and c) FFT of B_{ydq0} ; offset of Hall effect sensor "*a*", $\Delta B_{ay} = 0.1 pu$. Machine operating condition: ω_r=1pu and i_{dq}=0pu, 1 PM demagnetized by 50%.

Fig. 11 shows the same results as Fig. 10 but when *Δk_a*=0.1 pu, *Δk_b*=0.05 pu and *Δk_c*=0 pu. The additional harmonic component at 1ω_r (harmonic order=1) is readily visible; which affect to the peak-peak of B_{ydq0} . A pre-commissioning stage to calibrate the sensors could be used if the signal processing is based on absolute measurements. On the contrary, they will not affect to the mean value of B_{ydq0} . For the Hall-effect sensors used in this work [30], the error in the gains is <0.01pu.

As for the case of DC offsets, unbalances in the sensors' gains are not expected to affect to the performance of the method if demagnetization is based incremental instead of absolute measurements.

V.C. Influence of manufacturing tolerances

Tolerances during sensors assembling include displacements in axial, radial and angular directions.

Axial and radial displacements will produce the same affects as unbalances in sensor's gains already analyzed [18].

Angular displacements of the sensors, φ_{disp_a} , φ_{disp_b} and φ_{disp_c} , can be modeled as (10). Using some basic trigonometric transformations (10) can be expressed as (11), where $\Delta B_{\varphi_{disp}}$ and φ_{disp} are the magnitude and phase of the induced harmonic component due to angular displacements of the sensors.

$$B_{mdq0} = 1/3\left(B_{mas}e^{j\left(\varphi_{disp\_a}\right)} + B_{mbs}e^{j\left(\varphi_{disp\_b}\right)} + B_{mcs}e^{j\left(\varphi_{disp\_c}\right)}\right) \quad (10)$$

$$B_{mdq0} = 1/3\left(B_{ma} + B_{mb} + B_{mc}\right) + \Delta B_{\varphi_{disp}}\sin\left(\omega_r t + \varphi_{disp}\right) \quad (11)$$

Fig. 12 shows the same results as Fig. 10 but when $\varphi_{disp\_a} = 0.078$ mechanical radians. It can be observed that an angular displacement of Hall sensor "*a*" (see Fig. 1) results in
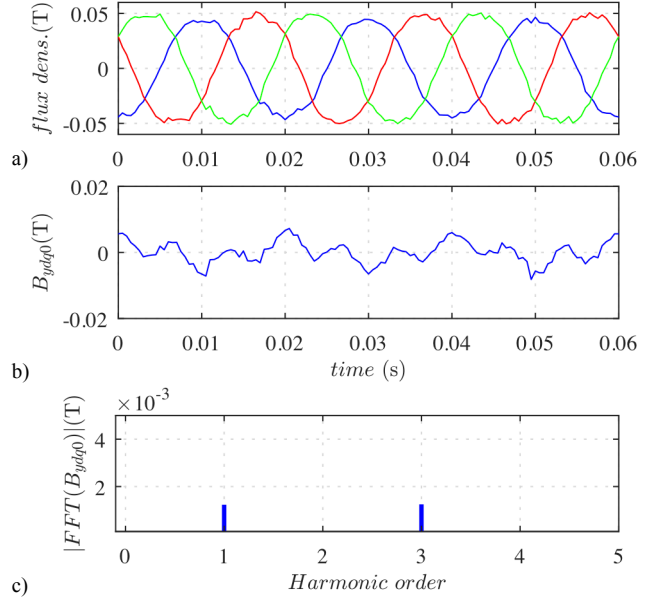

Fig. 11.- Same results as Fig. 10 but when *Δk_a*=0.1 pu, *Δk_b*=0.05 pu and *Δk_c*=0 pu.
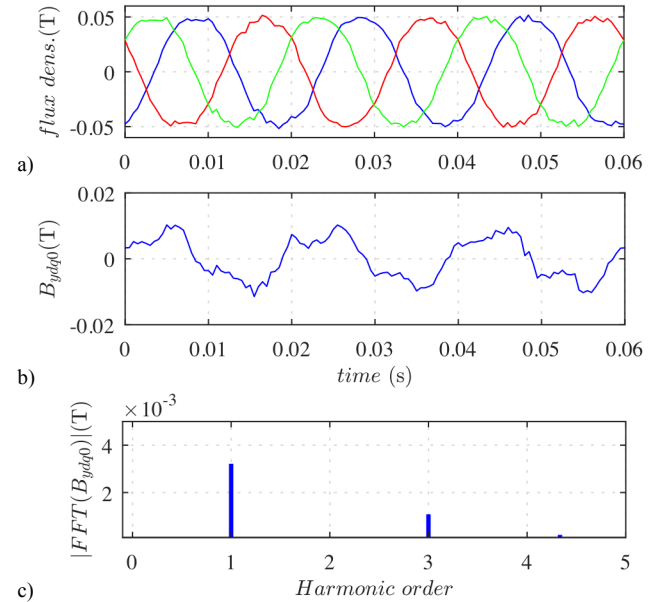

Fig. 12.- Same results as Fig. 10 but when $\varphi_{disp\_a} = 0.078$ rad.

an additional harmonic component at 1ω_r (harmonic order=1). This harmonic component does not affect to the mean value of B_{ydq0} , but it will affect to the peak-peak of B_{ydq0} and to the mean value of $\left| B_{ydq0}\right|$.

As discussed before, if demagnetization detection is based on incremental measurements with respect to the healthy case, angular displacements of the sensors are expected to have no influence.

V.D. Effects due to stator current

Negative *d*-axis fundamental current (flux-weakening current) will produce two different effects:
1) Reduce the magnetic flux density measured by the Hall-effect sensor, i.e. the field resulting by the *d*-axis
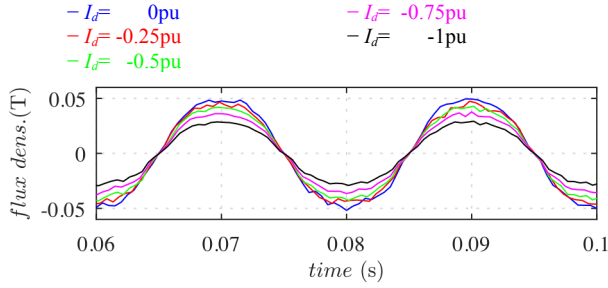
Fig. 13.- Flux density measurements in the *y*-axis direction by Hall-effect sensor "*a*", see Fig. 1. Machine operating condition: ω_r=1pu and I_q=0pu.

fundamental current will be superimposed to the PMs field. Fig. 13 shows the magnetic flux density measured in *y-axis* direction by Hall-effect sensor "*a*" (see Fig. 1), when negative *d*-axis current is applied and *q*-axis current is equal to zero. As expected, negative *d*-axis current reduces the magnetic flux density measured by the Hall-effect sensor [18]; the same effect will occur for all the sensors since the field resulting by the stator *d*-axis current is balanced, consequently, *d*-axis current virtually has no effect on B_{mdq0}.

2) Increase the harmonic content of the airgap flux [38]-[40] and therefore of the measurements of the Hall-effect sensor. It is observed from Fig. 13 that field-weakening current do not increase the harmonic content of the measurements for this particular machine. However, this conclusion cannot be generalized, the behavior is expected to be affected by stator/rotor configuration [41]-[43]. Decoupling of specific harmonics for each machine design (by means of look-up table, filtering …) might be needed in this case. This is a subject which requires further research.

Q-axis current produces a small shift of the measurement in all the three sensors with respect the no-current case, as well as an increase of their harmonic content [18]. The method performance will not be affected therefore by *q*-axis current injection.

V.E. Effects due to changes in magnets temperature

An increase of PMs' temperature results in a reduction of their remanent flux density. If the temperature of the PMs is uniform, the effect would be equivalent to injection of d-axis current discussed in section *V-D*. On the contrary, if the temperature of the rotor magnets were not uniform, the effect would be similar to those of a non-uniform demagnetization [18]. Both cases have been discussed in the preceding sections.

VI. Comparative analysis between demagnetization detection using the complex vector vs. the zero-sequence of magnetic flux density

Performance of the proposed method is compared with the method based on the magnetic flux density complex vector reported in [18].
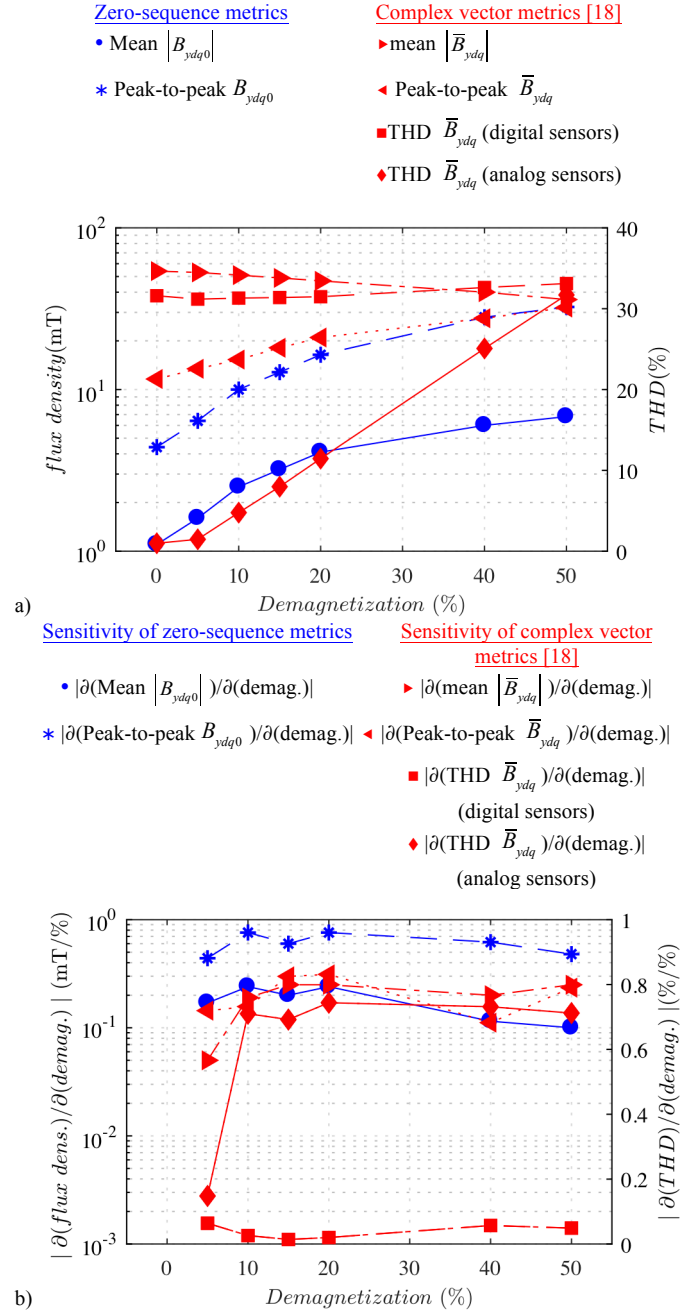

a)

b)

Fig. 14.- Comparative analysis of zero sequence based metrics proposed in this paper and complex vector based metrics proposed in [18]. a) Magnitude; b) variation of magnitude with magnetization (sensitivity). Machine operating condition: ω_r=1pu and i_{dq}=0pu.

Fig. 14 compares several metrics using both the zero-sequence magnetic flux density and the magnetic flux density complex vector, when demagnetization of PM #4 goes from zero (fully magnetized PM) to 50%; a logarithmic scale was found to provide a cleared representation of all metrics. Fig. 14a shows the variation of $\left|B_{ydq0}\right|$ and $\left|\overline{B}_{ydq}\right|$ (see [18]) and of the peak-to-peak of B_{ydq0} and $\overline{B}_{ydq}$ (see [18]), while Fig. 14b shows the absolute values of sensitivities to demagnetization of the metrics shown in Fig. 14a. It can be observed that the peak-to-peak of B_{ydq0} shows higher sensitivity to demagnetization than the magnetic flux density complex

vector metrics, while the mean of $\left|B_{ydq0}\right|$ shows higher sensitivity to demagnetization than the magnetic flux density complex vector metrics in the low demagnetization region. Fig. 14 also includes the variation of the THD of $\bar{B}_{ydq}$ when using analog and digital Hall-effect sensors (see [18]) and the sensitivities to demagnetization of these two metrics. Note that the THD cannot be used for the zero-sequence case, as no fundamental component exists (i.e. infinite THD). It is observed that the sensitivities to demagnetization, in the low demagnetization region, of $\left|B_{ydq0}\right|$ and peak-to-peak of B_{ydq0} are higher than the THD of $\bar{B}_{ydq}$ both with analog and digital Hall-effect sensors.

It is finally noted that THD based metrics are significantly more difficult to implement in terms of computational burden than metrics based on peak-to-peak or mean values, this also needs to be considered for the fair assessment of the different methods.

VII. Conclusions

Demagnetization detection based on the zero-sequence magnetic flux measurement has been analyzed in this work. The method uses standard Hall-effect sensors that are normally present in PMSMs drives for motion control, and can be implemented therefore without additional hardware requirements. Extensive experimental results have been provided to validate the proposed method. It has been shown that simple metrics as the peak-to-peak value or the mean value of the zero-sequence magnetic flux density can provide reliable estimations of the magnetization state. Discussion of issues affecting to the performance of the proposed method, including offsets in the sensors, unbalances of in sensors gains, PMs' temperature, manufacturing tolerances and stator current injection has been provided; In all these aspects, the proposed method shows a reduced sensitivity compared to the use of the flux density complex vector reported in [18]. Furthermore, all these implementation concerns virtually disappear if incremental instead of absolute measurements are used.

VIII. References

[1] J. F. Gieras and M. Wing, "Permanent magnet motor technology: design and application". Second edition 2002.

[2] D. W. Novotny and T. A. Lipo, "Vector Control and Dynamics of AC Drives," Oxford Science Publications, 1996.

[3] K. Akatsu, M. Arimitsu, and S. Wakui, "Design and control of a field intensified interior permanent magnet synchronous machine," IEEJ Trans. Ind. Appl., 126(7): 827–834, Jul. 2006.

[4] D. Reigosa, F. Briz, M. W. Degner, P. García and J. M. Guerrero, "Magnet temperature estimation in surface PM machines during six-Step operation". IEEE Trans. on Ind. Appl., 48(6): 2353–2361, Nov.-Dec. 2012.

[5] D. Reigosa, F. Briz, M. W. Degner, P. García and J. M. Guerrero, "Temperature issues in saliency-tracking-based sensorless methods for PM synchronous machines". IEEE Trans. on Ind. Appl., 47(3): 1352–1360, May-June 2011.

[6] D. Reigosa, D. Fernandez, H. Yoshida, T. Kato and F. Briz "Permanent-Magnet Temperature Estimation in PMSMs Using Pulsating High-Frequency Current Injection," IEEE Trans. on Ind. Appl., 51(4): 3159–3168, July-Aug 2015.

[7] N. Limsuwan, T. Kato, K. Akatsu, and R. D. Lorenz, "Design and evaluation of a variable-flux flux-intensifying interior permanent-magnet machine," IEEE Trans. Ind. Appl., 50(2): 1015–1024, Mar./Apr. 2014.

[8] Athavale, K. Sasaki, B. S. Gagas, T. Kato, and R. D. Lorenz, "Variable Flux Permanent Magnet Synchronous Machine (VF-PMSM) Design Methodologies to Meet Electric Vehicle Traction Requirements with Reduced Losses," IEEE Trans. Ind. Appl., 53(5): 4318–4326, Sep./Oct. 2016.

[9] S. Ruoho, J. Kolehmainen, J. Ikaheimo and A. Arkkio,"Interdependence of Demagnetization, Loading, and Temperature Rise in a Permanent-Magnet Synchronous Motor," IEEE Trans. Magn., vol. 46, no. 3, pp. 949–953, Mar. 2010.

[10] J Hong, D Hyun, and S.B.Lee, "Automated monitoring of magnet synchronous motors at standstill," IEEE Trans. Ind. Appl., 46 (4): 1397 - 1405, 2010 .

[11] IEC 62. 2-2004., "IEEE guide for diagnostic field testing of electric power apparatus-electrical machinery," 2004.

[12] D. Fernandez, D. Reigosa, T. Tanimoto, T. Kato, and F. Briz, "Wireless permanent magnet temperature & field distribution measurement system for IPMSMs," IEEE ECCE, pp. 3996–4003, Sep. 2015.

[13] X. Xiao, C. Chen and M. Zhang, "Dynamic Permanent Magnet Flux Estimation of Permanent Magnet Synchronous Machines", IEEE Trans. on Appl. Sup., 20(3): 1085–1088, June. 2010.

[14] K. Liu and Z. Q. Zhu "Online Estimation of the Rotor Flux Linkage and Voltage-Source Inverter Nonlinearity in Permanent Magnet Synchronous Machine Drives," IEEE Trans. on Pow. Elect., 29(1): 418-427, Jan. 2014.

[15] K. Liu, Q. Zhang, J. Chen, Z. Q. Zhu, and J. Zhang, "Online multiparameter estimation of nonsalient-pole PM synchronous machines with temperature variation," IEEE Trans. Ind. Electron., vol. 58, no. 5, pp. 1776–1788, May 2011.

[16] D. Reigosa, D. Fernandez, J. M. Guerrero, Z.Q. Zhu and F. Briz, "PMSM Magnetization State Estimation Based on Stator-reflected PM Resistance Using High Frequency Signal Injection", IEEE Trans. on Ind. Appl., 51(5): 3800-3810, Sept.-Oct. 2015.

[17] D. Fernandez, D. Reigosa, Z.Q. Zhu and F. Briz, "Permanent-Magnet Magnetization State Estimation Using High-Frequency Signal Injection", IEEE Trans. on Ind. Appl., 52(4): 2930-2949, July-Aug. 2016.

[18] D. Reigosa, D. Fernandez, Yonghyun Park, A. B. Diez, S. B. Lee and F. Briz, "Detection of Demagnetization in Permanent Magnet Synchronous Machines using Hall-Effect Sensors" IEEE Trans. on Ind. Appl., 54(4): Early Access, 2018. DOI: 10.1109/ECCE.2017.8096799.

[19] J.-R. R. Ruiz, A. G. Espinosa, L. Romeral, and J. Cusidó, "Demagnetization diagnosis in permanent magnet synchronous motors under non-stationary speed conditions," Electr. Power Syst. Res., 80(10): 1277–1285, Oct. 2010.

[20] S. Rajagopalan, W. le Roux, T. G. Habetler, and R. G. Harley, "Dynamic eccentricity and demagnetized rotor magnet detection in trapezoidal flux (brushless DC) motors operating under different load conditions," IEEE Trans. Power Electron., 22(5): 2061–2069, Sep. 2007.

[21] C. Urresty, J.-R. R. Ruiz, M. Delgado, and L. Romeral, "Detection of demagnetization faults in surface-mounted permanent magnet synchronous motors by means of the zero-sequence voltage component," IEEE Trans. Energy Convers., 27(1): 42–51, Mar. 2012.

[22] J. C. Urresty, J.-R. R. Ruiz, and L. Romeral, "A back-EMF based method to detect magnet failures in PMSMs," IEEE Trans. Magn., 49(1): 591–598, Jan. 2013.

[23] Z. Yang, X. Shi, and M. Krishnamurthy, "Vibration monitoring of PM synchronous machine with partial demagnetization and inter-turn short circuit faults," in Proc. IEEE ITEC, pp. 1–6, June 2014.

[24] D. Torregrossa, A. Khoobroo and B Fahimi, "Prediction of Acoustic Noise and Torque Pulsation in PM Synchronous Machines With Static Eccentricity and Partial Demagnetization Using Field Reconstruction Method", IEEE Trans. on Ind. Elect., 59(2): 934–944, Feb. 2012.

[25] J. C. Urresty, R. Atashkhooei, J.-R. R. Ruiz, L. Romeral, and S. Royo, "Shaft trajectory analysis in a partially demagnetized permanent-magnet synchronous motor," IEEE Trans. Ind. Electron., 60(8): 3454–3461, Aug. 2013.

[26] J. Hong, D. Hyun, S.B. Lee, J.Y. Yoo and K.W. Lee, "Automated Monitoring of Magnet Quality for Permanent-Magnet Synchronous

Motors at Standstill," IEEE Trans. Ind. Appl., 46(4): 1397–1405, July-Aug. 2010.

[27] Maxonmotorusa.com, "maxon sensor - Key information," Mar. 23, 2017. [Online]. Available: http://www.maxonmotorusa.com/

[28] Siemens.com, "Three-phase synchronous motors based on permanent magnet technology," Catalog D 86.2 • 2007, Mar. 23, 2017. [Online]. Available: http://w3.siemens.com/mcms/mc-solutions/en/motors/

[29] L. Xiao, Y. Yunyue, Z. Zhuo, "Study of the Linear Hall-Effect Sensors Mounting Position for PMLSM," IEEE Conference on Industrial Electronics and Applications, pp. 1175 – 1178, May 2017.

[30] http://www.allegromicro.com/en/Products/Magnetic-Linear-And-Angular-Position-Sensor-ICs/Linear-Position-Sensor-ICs/A1301-2.aspx

[31] D. Reigosa, D. Fernandez, M. Martinez, Y. Park, S. B. Lee and F. Briz, "Permanent Magnet Synchronous Machine Non-Uniform Demagnetization Detection Using Zero-Sequence Magnetic Field Density," IEEE ECCE'18, pp. 769 – 775, Sept. 2018.

[32] J. C. Urresty, R. Atashkhooei, J. R. Riba, L. Romeral and S. Royo, "Shaft Trajectory Analysis in a Partially Demagnetized Permanent-Magnet Synchronous Motor." IEEE Transactions on Industrial Electronics, vol. 60, no. 8, pp. 3454-3461, Aug. 2013.

[33] B. H. Lam, S. K. Panda, J. X. Xu and K.W. Lim "Torque ripple minimization in PM synchronous motor using iterative learning control", IEEE PED, pp. 141-149, 1999.

[34] A. Houari, F. Auger, J-C. Olivier and M. Machmoum, "A New Compensation Technique for PMSM Torque Ripple Minimization", IEEE IAS, pp. 1-6, Oct. 2015.

[35] C. Lai, G. Feng, K. Mukherjee, V. Loukanov and N. C. Kar, "Torque ripple minimization for interior PMSM with consideration of magnetic saturation incorporating on-line parameter identification", IEEE CEFC, Jan. 2017.

[36] G. Feng, C. Lai, J. Tian and N. C. Kar, "Multiple Reference Frame based Torque Ripple Minimization for PMSM Drive Under Both Steady-State and Transient Conditions ", IEEE Trans. on Power Elect., Dec. 2018 (early access).

[37] https://www.ansys.com

[38] Q. Li, T. Fan, X. Wen, and P. Ning, "An Analytical approach to magnet eddy-current losses for interior permanent-magnet synchronous machines during flux weakening," IEEE Trans. Magnet, 51(8): 1–9, Aug. 2015.

[39] Z. Q. Zhu, Y. S. Chen, and D. Howe, "Iron loss in permanent-magnet brushless AC machines under maximum torque per ampere and flux weakening control," IEEE Trans. Magnet., 38 (5): 3285–3287, Sep. 2002.

[40] K. Akatsu, K. Narita, Y. Sakashita and T. Yamada "Impact of flux weakening current to the iron loss in an IPMSM including PWM carrier effect," IEEE ECCE, pp. 1927-1932, Sept. 2009.

[41] M. Barcaro, N. Bianchi and F. Magnussen, "Rotor Flux-Barrier Geometry Design to Reduce Stator Iron Losses in Synchronous IPM Motors Under FW Operations," IEEE Trans. on Ind. Appl., 46:(5), 928–935, July 2010.

[42] A. E. Fitzgerald, C. Kingsley. S. D. Umans,"Electric Machinery". Sixth Edition, Mc Graw Hill, 2003.

[43] J. Pyrhönen, T. Jokinen, V. Hrabovcová, "Design of Rotating Electrical Machines". Wiley, 2008.